Journal of Medicinal Chemistry Article

J. Med. Chem. **2010,** *53,* 7287–7295 **7287**
DOI: 10.1021/jm100812a

Design, Synthesis, and Evaluation of Indolinones as Inhibitors of the Transforming Growth Factor β Receptor I (TGFβRI)†

Gerald J. Roth,*[,‡] Armin Heckel,[‡] Trixi Brandl,[#,‡] Matthias Grauert,[‡] Stefan Hoerer,[§] Joerg T. Kley,[‡] Gisela Schnapp,[§] Patrick Baum,[∥] Detlev Mennerich,[∥,⊥] Andreas Schnapp,[∥] and John E. Park[∥]

[‡]*Biberach, Department of Medicinal Chemistry,* [§]*Biberach, Department of Lead Discovery, and* [∥]*Biberach, Department of Pulmonary Diseases Research, Boehringer Ingelheim Pharma GmbH & Co. KG, Birkendorfer Strasse 65, D-88397 Biberach, Germany, and* [⊥]*Boehringer Ingelheim Pharmaceuticals Inc., Ridgefield, Connecticut, United States.* [#]*New address: Novartis Institutes for BioMedical Research, Novartis Pharma AG, Basel, Switzerland.*

Received March 10, 2010

Inhibition of transforming growth factor β (TGFβ) type I receptor (Alk5) offers a novel approach for the treatment of fibrotic diseases and cancer. Indolinones substituted in position 6 were identified as a new chemotype inhibiting TGFβRI concomitant with a low cross-reactivity among the human kinome. A subset of compounds showed additional inhibition of platelet-derived growth factor receptor alpha (PDGFRα), contributing to an interesting pharmacological profile. In contrast, p38 kinase, which is often inhibited by TGFβRI inhibitors, was not targeted by derivatives based on the indolinone chemotype. Guided by an X-ray structure of lead compound **5** (BIBF0775) soaked into the kinase domain of TGFβRI, optimization furnished potent and selective inhibitors of TGFβRI. Potent inhibition translated well into good inhibition of TGFβRI-mediated phosphorylation of Smad2/3, demonstrating efficacy in a cellular setting. Optimized compounds were extensively profiled on a 232-kinase panel and showed low cross-reactivities within the human kinome.

Introduction

Transforming growth factor β (TGFβ[a]) is a pluripotent cytokine involved in the regulation of various biological processes such as cell proliferation, differentiation, migration, adhesion, apoptosis, and epithelial-to-mesenchymal transition (EMT).[1] TGFβ signaling is linked to the pathology of numerous diseases.[2] Therapeutic approaches to inhibit its signaling by targeting TGFβ receptor I (TGFβRI) with antibodies, antisense molecules, or kinase inhibitors[3] are widely discussed for the treatment of idiopathic pulmonary fibrosis (IPF) and cancer.[4,5] Lung diseases like asthma, chronic obstructive pulmonary disease (COPD), or IPF are associated with an abnormal inflammatory response in combination with airway remodeling through fibrosis, goblet cell hyperplasia, and smooth muscle thickening.[4,6] Among other growth factors and cytokines, TGFβ, highly expressed in fibrotic tissues, upregulates the expression of adhesion molecules required for the recruitment of monocytes and neutrophils which both initiate inflammatory responses. Furthermore, TGFβ plays a pivotal role in the biosynthesis and turnover of extracellular matrix (ECM) proteins like collagens, fibronectin, and proteoglycans and is thus contributing to fibrosis and stimulation of smooth muscle cell proliferation,[7] suggesting that inhibition of TGFβ signaling may provide a therapeutic potential in diseases like asthma and COPD. During cancerogenesis, the function of TGFβ is Janus-faced. On the one hand, TGFβ acts as tumor suppressor by inhibiting the proliferation of normal epithelial, endothelial hematopoietic cells, and early epithelial cancer cells. On the other hand, once tumorigenesis has been initiated, tumor cells escape this growth control and produce high levels of TGFβ, resulting in profound changes of the tumor's microenvironment in which TGFβ promotes tumor growth. The tumor-promoting effects include extracellular matrix degradation and EMT by increased production of platelet-derived growth factor (PDGF), connective tissue growth factor (CTGF), and matrix metalloproteinases (MMPs). Furthermore, angiogenesis is induced by an upregulation of vascular endothelial growth factor (VEGF).[5,8]

Clearly, inhibition of TGFβRI holds promise as a new modality for the treatment of fibrotic diseases and cancer. Several small molecules targeting TGFβRI have been reported in literature (see Chart 1),[3] among them SB-431542 **1a**,[9] SB-505124 **1b**,[9] LY-2109761 **2**,[10] SM-16 **3**,[11] SD-208 **4**,[12] and others.[8b,13−15] LY-2157299, a derivative of compound **2**, was advanced into phase I clinical trials for the treatment of cancer.[16] Most of the known

†The atomic coordinates for the X-ray structure of compound **5** soaked into the kinase domain of TGFβRI have been deposited in the Protein Data Bank, PDB code 2x7o.

*To whom correspondence should be addressed. Phone: +49-7351-540. Fax: +49-7351-540. E-mail: gerald.roth@boehringer-ingelheim.com.

[a] Abbreviations: TGFβ, transforming growth factor betaβ; TGFβR, transforming growth factor beta receptor; PDGF, platelet-derived growth factor; PDGFR, platelet-derived growth factor receptor; VEGF, vascular endothelial growth factor; Smad, SMA/MAD-related protein family; BMPR2, bone morphogenetic protein receptor type 2; Alk, activin receptor-like kinase; ECM, extracellular matrix; EMT, epithelial-to-mesenchymal transistion; IPF, idiopathic pulmonary fibrosis; COPD, chronic obstructive pulmonary disease; CTGF, connective tissue growth factor; MMP, matrix metalloprotease; TBTU, *O*-(benzotriazol-1-yl)-*N*,*N*,*N*′,*N*′-tetramethyluronium tetrafluoroborate; HOBt, hydroxybenzotriazole; ROE, rotating frame Overhauser enhancement; Pampa, parallel artificial membrane permeability assay.

Published on Web 10/04/2010

Chart 1. TGFβRI Inhibitors

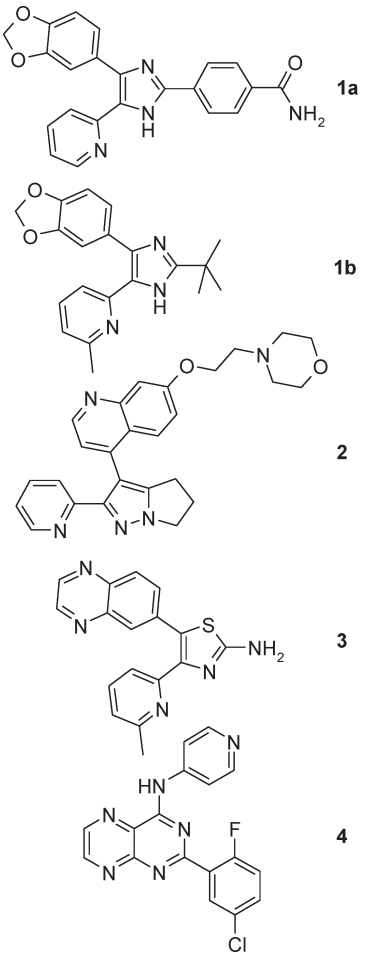

Chart 2. TGFβRI Hit Compound **5** and General Structure **6**

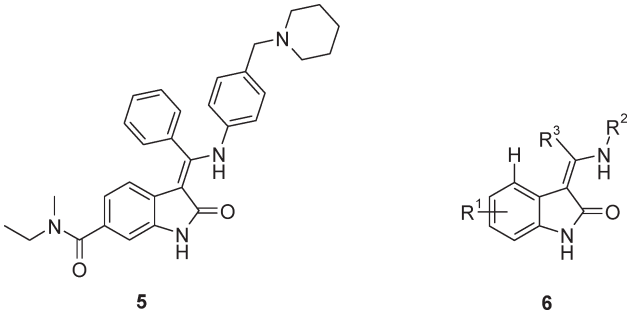

TGFβRI inhibitors are based on five-membered heterocyclic chemotypes (imidazoles, pyrazoles, or thiazoles, compounds **1**−**3**) typically interacting with the kinase hinge region by one single hydrogen acceptor.

In this paper, we report the identification of indolinones as a novel chemotype for the inhibition of TGFβRI, broadening the repertoire of TGFβRI (Alk5) kinase inhibitor scaffolds. Optimization of an initial lead **5** (BIBF0775, Chart 2)[18] led to compounds showing potent TGFβRI inhibition with low cross-reactivity in the human kinome.

Chemistry

Various approaches for the synthesis of the compounds described in Tables 1−3 were developed. The particular synthetic route was dependent on the specific point of diversification to be addressed during synthesis. To that end, building blocks **10**, **11**, **15**, **22**, and **23** were designed and synthesized by the methods mentioned below (see Scheme 1).

Table 1. TGFβRI/pSmad Inhibition of Substituted Indolinones

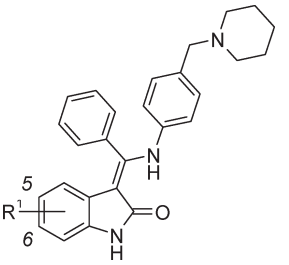

compound	R^1	TGFβRI IC_{50} (nM) [a]	pSmad EC_{50} (nM) [a]
5	6-CONEtMe	34 ± 30	105 ± 70
35	6-CONH(CH_2CH_3)	24 ± 17	75 ± 53
36	6-CONHCH_3	32 ± 26	NT [b]
37	6-CONMe_2	35 ± 22	246 ± 130
38	6-CONH*n*Bu	91 ± 49	1065 ± 588
39	6-(pyrrolidine-1-carbonyl)	245 ± 170	696 ± 542
40	6-CONH*i*Pr	318 ± 188	708 ± 453
41	6-CONH_2	369 ± 213	>50000
42	6-CONH(CH_2CH_2OH)	430 ± 227	>50000
43	6-CONEt_2	625 ± 396	NT [b]
44	6-CONHBn	1532 ± 908	NT [b]
45	H	3462 ± 2621	NT [b]
46	5-CONMe_2	186 ± 104	198 ± 111
1a (SB-431542)[c]		125 ± 65	172 ± 108

[a] Values are averages ± SD of at least three independent determinations. Values "greater than (>)" indicate that half-maximum inhibition was not achieved at the highest concentration tested. All compounds showed good solubility (>10 μM) in the assay buffers. [b] Not tested. [c] See ref 9.

N-Acetylated indolinones **16** and **17** were condensed with *ortho*-benzoic acid triethyl ester to furnish intermediates **18** and **19**.[17,18] The 3-ethoxymethylene unit is suitable to undergo addition−elimination reactions. Consequently, compounds **18** and **19** were reacted with amines according to previously published protocols[18] to yield intermediates **20** and **21** after subsequent acetyl cleavage. The resulting methyl esters were hydrolyzed to get access to carboxylic acids **22** and **23** used as building blocks suitable for diversification of position R^1.

For diversification in position 3 of the indolinones, 3-hydroxymethylene substituted derivatives had to be used as building blocks, which in contrast to the 3-ethoxymethylene substituted compounds are not susceptible to hydrolysis during the subsequent saponification step. To introduce the hydroxymethylene functionality, *N*-acetylated indolinone **7** was directly condensed with benzoic acid after TBTU activation. Compound **8** was hydrolyzed to yield carboxylic acid **9**. Amide coupling using ethylamine or *N*-methyl ethylamine furnished building blocks **10** and **11**. Building block **15** was synthesized in a similar fashion. Formic acid ethyl ester was used to introduce the 3-hydroxymethylene moiety in this case.

The final compounds were synthesized by two different procedures. Whenever diversification of position R^1 was requested (see Chart 2), amide coupling with the respective amine using building blocks **22**, **23**, **25**,[18] and **28**[18] was the obvious method of choice. For diversification of position R^2 in the final step, a new synthetic protocol had to be developed directly utilizing the hydroxymethylene functionality of building blocks **10**, **11** and **15**. We envisaged a novel in situ activation of the alcohol moiety

Table 2. Inhibitory Profile of 6-Amido-Substituted Indolinones

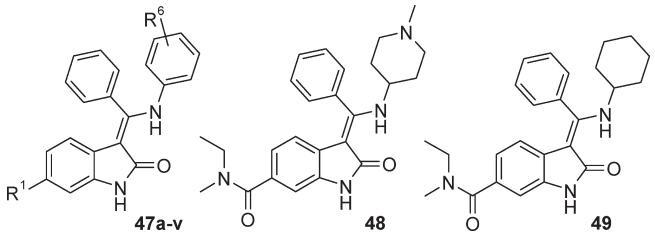

compd	R^1	R^6	IC_{50} (nM) TGFβRI[a]	IC_{50} (nM) PDGFRα[b]	EC_{50} (nM) pSmad[c]
47a	CONHEt	4-$(NSO_2CH_3)(CH_2)_2NMe_2$	1 ± 1	74	108 ± 65
47b	CONEtMe	4-$(NSO_2CH_3)(CH_2)_2NMe_2$	7 ± 5	155	209 ± 108
47c	CONHEt	4-$(NCOCH_3)(CH_2)_2NMe_2$	3 ± 3	130	1066 ± 659
47d	CONEtMe	4-$(NCOCH_3)(CH_2)_2NMe_2$	8 ± 5	160	102 ± 61
47e	CONHEt	4-$(NCOCH_3)(CH_2)_3NMe_2$	3 ± 3	59	1249 ± 664
47f	CONEtMe	4-$(NCOCH_3)(CH_2)_3NMe_2$	9 ± 6	176	411 ± 309
47g	CONHEt	4-$(NCH_3)COCH_2$−(4-methyl-piperazin-1-yl)	9 ± 11	107	1370 ± 735
47h	CONEtMe	4-$(NCH_3)COCH_2$−(4-methyl-piperazin-1-yl)	7 ± 6	1972	833 ± 549
47i	CONHEt	4-CH_2NMe_2	19 ± 13	99	185 ± 99
35	CONHEt	4-CH_2(piperidin-1-yl)	24 ± 17	789	75 ± 53
5	CONEtMe	4-CH_2(piperidin-1-yl)	34 ± 30	890	105 ± 70
47j	CONHEt	4-$(NCH_3)COCH_2NMe_2$	35 ± 22	137	3383 ± 3291
47k	CONEtMe	4-$(NCH_3)COCH_2NMe_2$	29 ± 16	367	382 ± 207
47l	CONEtMe	4-CH_2NHEt	32 ± 18	1100	160 ± 83
47m	CONHEt	4-$CONH(CH_2)_2NEt_2$	33 ± 23	335	505 ± 264
47n	CONEtMe	4-$CONH(CH_2)_2NEt_2$	64 ± 53	317	542 ± 317
47o	CONHEt	4-$(CH_2CH_2)NMe_2$	47 ± 27	368	135 ± 70
47p	CONEtMe	4-$(CH_2CH_2)NMe_2$	64 ± 40	420	259 ± 190
47q	CONEtMe	4-$(NSO_2CH_3)CH_2CONMe_2$	86 ± 53	410	>3000
47r	CONEtMe	4-$(NCH_3)SO_2Me$	231 ± 129	640	>10000
47s	CONEtMe	3-CH_2NEt_2	616 ± 353	1650	NT[d]
47t	CONEtMe	4-COOH	782 ± 435	564	NT[d]
47u	CONEtMe	4-$COOCH_3$	1970 ± 1085	1126	NT[d]
47v	CONEtMe	H	2586 ± 1844	>5000	NT[d]
48			>50000	>5000	>10000
49			>50000	>5000	>10000

[a] Values are averages ± SD of at least three independent determinations. Values "greater than (>)" indicate that half-maximum inhibition was not achieved at the highest concentration tested. All compounds showed good solubility (>10 μM) in the assay buffers. [b] IC_{50} values for PDGFRα are single determinations. [c] Values are averages ± SD of two−five independent determinations. Values "greater than" indicate that half-maximum inhibition was not achieved at the highest concentration tested. [d] Not tested.

Table 3. Inhibitory Profile of Various R^3-Substituted Indolinones

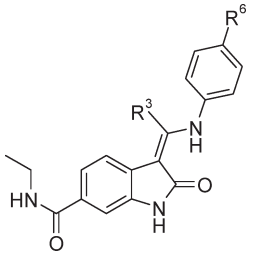

compd	R^3	R^6	IC_{50} (nM) TGFβRI[a]	IC_{50} (nM) PDGFRα[b]	EC_{50} (nM) pSmad[c]
47e	Ph	4-$(NCOCH_3)(CH_2)_3NMe_2$	3 ± 3	59	1249 ± 664
47w	H	4-$(NCOCH_3)(CH_2)_3NMe_2$	17 ± 10	484	597 ± 332
47g	Ph	4-$(NCH_3)COCH_2$−(4-methyl-piperazin-1-yl)	9 ± 11	107	1370 ± 735
47x	H	4-$(NCH_3)COCH_2$−(4-methyl-piperazin-1-yl)	15 ± 9	>5000	2175 ± 845
35	Ph	4-CH_2(piperidin-1-yl)	24 ± 17	789	75 ± 53
47y	H	4-CH_2(piperidin-1-yl)	69 ± 44	1292	376 ± 246
47j	Ph	4-$(NCH_3)COCH_2NMe_2$	35 ± 22	137	3383 ± 3291
47z	H	4-$(NCH_3)COCH_2NMe_2$	52 ± 30	2928	4355 ± 2298

[a] Values are averages ± SD of at least three independent determinations. [b] IC_{50} values for PDGFRα are single determinations. Values "greater than (>)" indicate that half-maximum inhibition was not achieved at the highest concentration tested. All compounds showed good solubility (>10 μM) in the assay buffers. [c] Values are averages ± SD of two to three independent determinations.

Scheme 1. Synthesis of Building Blocks[a]

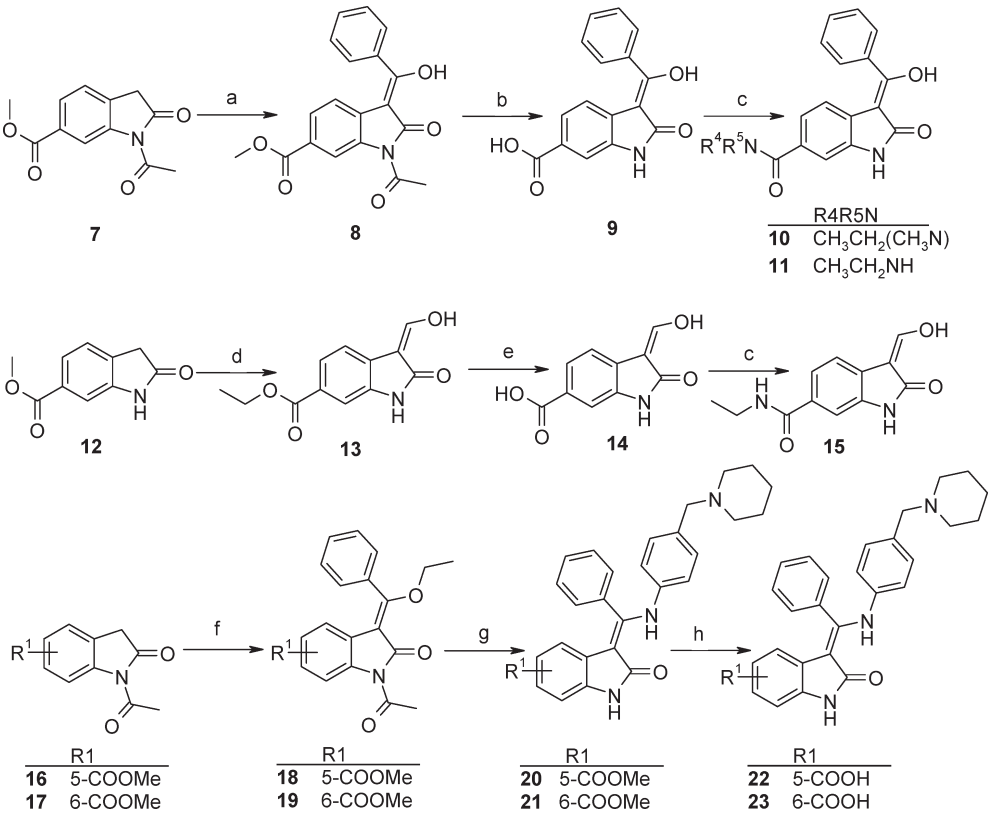

[a] (a) Benzoic acid, TBTU, NEt_3, NMP, rt; (b) 1N NaOH, MeOH, reflux; (c) $R^4R^5NH_2$, TBTU, HOBt, Huenig base or NEt_3, DMF, rt; (d) formic acid ethylester, NaOEt, EtOH, 80 °C; (e) 1N NaOH, EtOH, 80 °C; (f) $(EtO)_3CPh$, Ac_2O, 100 °C; (g) 4-piperidin-1-ylmethyl-phenylamine, DMF, 80 °C, then NH_3, 40 °C; (h) 1N NaOH, MeOH/dioxane, reflux.

as a convenient way for further derivatization. To that end, various methods for the condensation with amines were tested. Gratifyingly, heating compounds **10**, **11**, or **15** and amines R^2NH_2 under microwave irradiation after activation with trimethylsilyl imidazole turned out to be a successful process (probably via silylenolether formation), directly furnishing compounds **47a**−**z** in good yield (Scheme 2).

The double bond geometry in the final compounds **35**−**47** and in intermediates **8**−**11**, **13**−**15**, **18**, and **19** is locked in a *Z*-conformation by an intramolecular hydrogen bond.[18] This is proven by an ROE effect between the proton in position 4 of the indolinone core and the proton at the exocyclic double bond (**6**, R^3 = H) for several 3-methylene-substituted compounds (**13**−**15** and **47w**−**z**) and by an ROE effect between the proton in position 4 of the indolinone core and the proton in position 2 of the central aryl moiety (**6**, R^3 = Ph) for 3-phenylmethylene-substituted compounds (such as **5** or **8**−**11**). In addition, an upfield shift of the proton in position 4 of the indolinone core can be observed in all final compounds with a phenyl moiety in position R^3 of formula 6 due to magnetic shielding by the R^3-phenyl moiety.

Results and Discussion

To identify inhibitors of the TGFβ receptor I, a high-throughput screening of our internal compound collection was performed using a TGFβRI substrate phosphorylation assay.[19] Among the hits, compound **5** (Chart 2)[18] and a few additional indolinone derivatives (**36**, **37**, **40**, **41**, and **45**) were identified as a cluster displaying down to double-digit nanomolar potency in the TGFβRI assay (see Table 1). Since we knew from earlier kinase projects that inhibitors based on the indolinone chemotype can show low cross-reactivity among the human kinome,[18] we evaluated prototype **5** for potential cross-reactivities in a kinase selectivity panel. Among 30 kinases tested,[20] only two additional enzymes (MKK1 and MAPKAP kinase 1a) showed a slight inhibition in the screen (see Table 4). Notably, p38 kinase (often targeted by other TGFβRI inhibitors[5,8b]) was not inhibited. TGFβRII, BMPR2, and Alk1 (kinases with high homology to TGFβRI) were additionally tested. Compound **5** inhibited these kinases only in the micromolar range (IC_{50} TGFβRII 19 μM, IC_{50} BMPR2 >50 μM, IC_{50} Alk1 4 μM). Due to this promising selectivity profile, compound **5** was chosen as a starting point for further optimization.

X-ray crystallography was used to guide our optimization efforts. To that end, compound **5** was soaked into crystals of the kinase domain of TGFβRI. The X-ray structure (see Figure 1) confirms the typical binding mode of indolinones into known kinase ATP pockets displaying the canonical hydrogen bonds between the lactam moiety and the kinase hinge region. The 6-amido substituent on the indolinone core points toward the TGFβRI specificity pocket flanked by the gatekeeper Phe^{262} and Lys^{232}. We reasoned that the favorable selectivity profile of **5** may be attributable to the amido moiety binding into this part of the enzyme. On the other hand, the basic side chain of **5** points toward the water phase, suggesting a high degree of freedom for structural modifications in this region. The central phenyl moiety of **5** is situated in the part of the pocket that is occupied by the ribose moiety of ATP when bound.

We decided to explore the structure−activity relationships of indolinones substituted in positions R^1, R^2, and R^3 of

Scheme 2. Synthesis of Final Compounds[a]

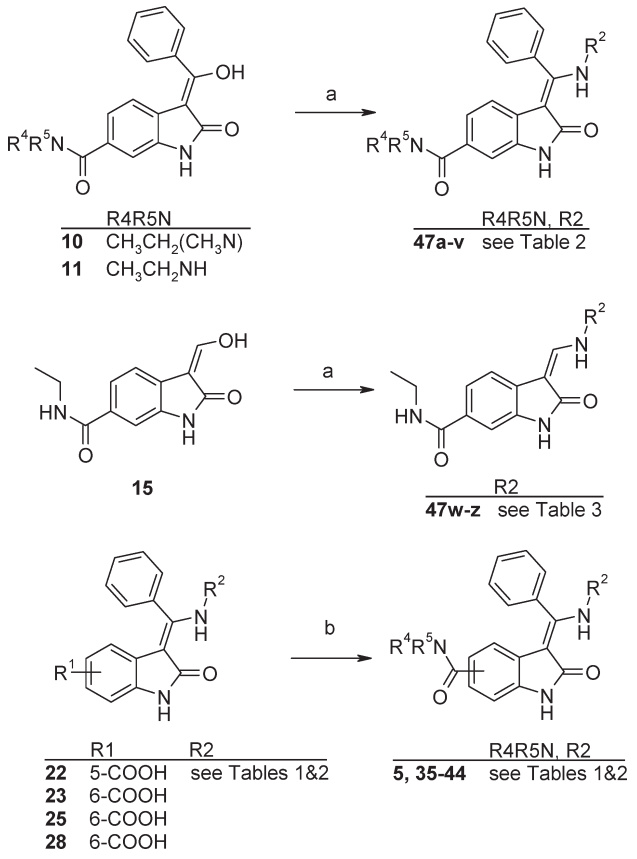

[a] (a) R^2NH_2, TMS-imidazole, THF, 170 °C, microwave; (b) $R^4R^5NH_2$, TBTU, HOBt, Huenig base or NEt_3, DMF, rt.

scaffold **6** (see Chart 2). In the first place, we aimed to evaluate the effects of substitutions at R^1 on TGFβRI potency as well as to confirm our hypothesis that selectivity versus other kinases was attributable to the 6-amido substitution. When comparing a number of differently substituted indolinone cores (see Table 1), it could clearly be seen that smaller secondary and tertiary amides (**5**, **35**−**38**) in position 6 were favorable for a good TGFβRI potency, whereas a drop of potency could be observed for primary amide **41** as well as larger amides **39**, **40**, and **42**−**44**. The unsubstitued indolinone **45** was significantly less active, confirming that the 6-amido substituents contribute to the overall binding energy. On the other hand, compound **45** tested at 1 μM concentration inhibited more than 50% of the kinases in the selectivity panel[20] mentioned before (Table 4). When shifting the amido substituent into position 5 (compare compounds **46** and **37**), TGFβRI inhibition is retained. However, compound **46** shows a less favorable selectivity profile versus other kinases (9 kinases inhibited at 1 μM compound concentration, see Table 4). This data confirmed that the 6-amido substitution is the decisive motif for a favorable selectivity profile as well as potent TGFβRI inhibition.

The compounds in Table 1 were also evaluated for their ability to inhibit the TGFβRI-mediated signal transduction in a cellular setting.[19] TGFβ receptors activated by TGFβ phosphorylate the receptor-regulated Smads for TGFβ, Smad2 and 3.[21] Therefore, a phospho Smad2/3 ELISA was established.[19] Because the phosphorylated Smad 2/3 proteins will undergo multimerization with the comediator Smad4 and will translocate into the nucleus to regulate the transcription of target genes

Table 4. Kinase Selectivity Profiles of Selected Compounds (% Remaining Kinase Activity in the Presence of 1 μM Test Compound)

compound	**5**	**45**	**46**	**47a**	**47i**	**47l**
AMPK	80[a]	***4***	***2***	74	85	81
CDK2/A	110	***38***	***39***	100	103	87
CHK1	74	***6***	***8***	51	84	85
CK1	108	***17***	95	100	102	90
CK2	98	90	73	94	95	86
CSK	72	***32***	74	83	96	78
DYRK1A	88	***18***	45	96	105	86
ERK2	96	77	95	104	98	87
GSK3b	82	***1***	***5***	124	114	56
MKK1A	***47***	***0***	***4***	80	93	50
MKK1	***48***	***4***	***12***	53	59	61
MKK2	102	75	94	NT[b]	NT[b]	97
MSK1	92	***8***	***36***	105	104	83
NEK2A	96	***39***	81	70	98	72
NEK6	88	86	87	118	123	92
p38α	92	96	91	110	121	85
p38β2	98	NT[b]	100	NT[b]	NT[b]	NT[b]
p38γ	93	NT[b]	91	NT[b]	NT[b]	NT[b]
p38δ	108	NT[b]	99	NT[b]	NT[b]	86
PBK	150	***5***	***19***	101	102	88
PDK1	109	***8***	71	102	89	89
PKA	96	***12***	69	75	90	96
PKB	97	88	93	90	106	92
PKCalpha	88	***29***	***28***	100	89	85
PRAK	87	***38***	59	67	96	70
ROCKII	88	54	79	88	95	80
S6K1	96	***12***	76	100	101	89
SAPK1c	89	***8***	90	105	99	91
Src[c]	86	NT[b]	NT[b]	NT[b]	86	61
SGK	123	***20***	68	107	124	106

[a] Compounds were tested at 1 μM concentration and 100 μM ATP concentration as described in ref 18. Data are expressed as percent remaining kinase activity in the presence of the inhibitors relative to control, which was 100% in the absence of inhibitors. The bold and italic numbers indicate values less than 50. [b] Not tested. [c] Tested at 2 μM compound concentration.

in cooperation with nuclear cofactors, this assay detects the inhibition of the first step of the TGFβ-mediated signaling cascade. In general, the trend for inhibition correlated with the data from the biochemical assay. The compounds were however less potent in this setting when compared to the biochemical TGFβRI inhibition (factor 3−12 for potent compounds). This cellular efficacy was not impaired by potential cytotoxic effects. The compounds **5** and **46** (as well as **47i**, **47l**, and **47p** from Table 2) were analyzed using Cellomics' Cytotox Assay kit I: cellular membrane integrity, nuclear fragmentation and density, and lysosomal mass were measured. None of the compounds showed significant signs of toxicity (IC_{50} > 1 μM) in this setting.[22] Taken together, due to their good potency on a biochemical as well as cellular level, the compounds looked promising as starting points for further optimization.

To further explore structure−activity relationships, the R^2 side chain (Chart 2) pointing toward the water phase was chosen for the next round of modifications (Table 2). In general, aryl groups substituted in position 4 were decisive for good potency in this position. Anilines with smaller substituents R^6 (refer to **47r** and **47u** as representative compounds) or without any substitution (compound **47v**) were less active compared to lead compound **5**, resembling the SAR of other indolinone-based kinase inhibitors.[18] In addition, neutral compounds were also clearly inferior (compare the representative compound **47q** with **47b**). We therefore decided to retain a basic functionality in position R^6. When evaluating

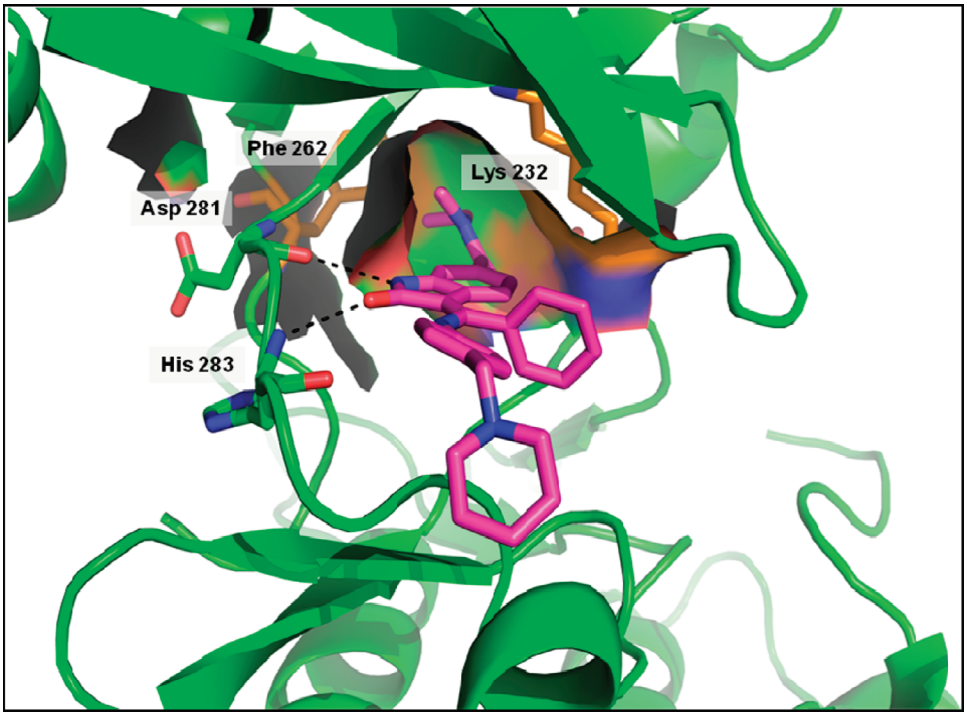

Figure 1. X-ray structure of compound **5** soaked into the kinase domain of TGFβRI. The canonical hydrogen bonds between the indolinone lactam moiety and Asp^{281} and His^{283} of the hinge region are highlighted, as is the gatekeeper Phe^{262} together with Lys^{232}.

various modifications, a high degree of freedom for structural variation of the charged side chain was observed. Various linkers between the aniline and the basic moiety were tolerated (**47a**−**u**). Also the distance between the amines and the core seemed to play a minor role demonstrating that structure−activity relationships in this respect were shallow. Attaching R^6 substituents on the aniline in position 3 rather than position 4 was also detrimental to activity (representative compound **47s**, Table 2). Replacing the aniline by saturated cyclic systems such as **48** and **49** led to complete loss of potency. Comparable to hit compounds **5** and **35**, indolinones substituted in position 6 with either an ethylamido or an ethylmethylamido substituent usually showed comparable activities with a tendency for higher potency for the ethylamido-substituted compounds (compare e.g. couples **47a/b**, **47c/d**, **47e/f**, etc). Although structure−activity relationships with respect to basic moieties were shallow, improved compounds with single-digit nanomolar TGFβRI inhibition could be identified by variation of position R^2, with compound **47a** showing an optimized IC_{50} of 1 nM.

Most compounds were also identified as inhibitors of the platelet-derived growth factor receptor kinase PDGFRα (see Table 2) as measured in a substrate phosphorylation assay.[19] Structure−activity relationships followed the same trend as observed for TGFβRI inhibition, the respective IC_{50} values were however higher when compared with TGFβRI inhibition. Because inhibition of PDGFR kinases has been reported as a therapeutic principle in the treatment of fibrotic diseases[19,23] and cancer[24] as well, we reasoned that additional inhibition of PDGFRα activity could contribute to an improved target profile of the compounds, potentially amplifying the overall efficacy in the treatment of diseases such as COPD and cancer.

Cellular efficacy of the compounds in Table 2 was again evaluated in the pSmad ELISA assay. For many compounds, EC_{50} values followed the same trend as mentioned before (see Table 1), i.e. cellular efficacy differed by a certain factor from biochemical IC_{50}. Disappointingly, however, many compounds of this series displayed increased shifts between cellular and biochemical inhibition. Among them, biochemically potent compounds such as **47c**, **47e**, **47g**, and **47h** showed cellular potency only with a >100-fold shift. As a possible explanation, the different basicity of the compounds could influence their permeability and cellular activitiy. Different pK_a values, however, cannot exclusively explain the variations seen, because even for compounds with higher basicity (such as **5** or **35**, pK_a = 9.2), the shift between biochemical and cellular activity is low. On the other hand, many of the compounds in Table 2 exerting lower cellular potency display clogP values[25] of less than 3.5. As an alternative explanation the increased polarity of the compounds could prevent them from permeating into the cells. This hypothesis was supported by permeability measurements of representative compounds: less polar compounds such as **5**, **35**, or **47i** (clogP > 3.6) show permeabilities in the range of 2.0×10^{-6} to 2.0×10^{-7} cm/s in a Pampa assay at pH 7.4, whereas for more polar compounds such as **47c**, **47e**, **47g**, and **47h** (clogP < 3.5) permeability values above 1.0×10^{-8} cm/s were obtained. Guided by this hypothesis, several optimized compounds with attractive cellular activities in the range of 100−200 nM such as **47a**, **47d**, **47i**, or **47l** were identified by balancing polarity and biochemical activity.

Finally, the influence of substitution at R^3 (Chart 2) was explored (see Table 3). When comparing compounds in which R^3 = phenyl with the corresponding compounds with R^3 = H (**47w**−**z**), a slight drop of potency could be observed for TGFβRI inhibition. This drop of potency was even more significant when comparing the PDGFRα inhibition of the respective couples. Therefore, derivatives without a central phenyl group offered the potential for increased selectivity versus PDGFRα (the potent TGFβRI inhibitor **47x**, for instance, was more than 300-fold selective versus PDGFRα). Because compounds **47w**−**z** (R^3 = H) are more polar than

their phenyl counterparts[25] (clogP < 3.0), poor cell permeability is probably again the reason for the low activity of the compounds in the pSmad ELISA assay. Only the more lipophilic compound **47y** (clogP = 3.4) showed improved cellular activity in this series.

Having optimized the TGFβRI inhibition of the initial lead, the most potent compound **47a** as well as indolinones **47i** and **47l** were again evaluated in our standard kinase selectivity panel (Table 4).[20] No single kinase was inhibited (<50% control) at 1 μM compound concentration. With this promising data as an indicator for a favorable cross reactivity profile, we were eager to learn how the picture would look like when testing the compounds on a larger panel of kinases. Compounds **5** and **47i** were therefore characterized in a panel of 232 kinases (Invitrogen) at 2 μM compound concentration.[26] The compounds retained a favorable cross reactivity profile (see Supporting Information), confirming our initial selectivity assessment. For each compound, a few additional enzymes were identified as targets (>90% inhibition at 2.0 μM and >50% inhibition when tested at 0.2 μM). In particular, compound **47i** (targeting 15/232 additional kinases at 0.2 μM) appeared to be slightly more selective in this panel when compared to compound **5** (targeting 20/232 additional kinases at 0.2 μM). The pharmacological consequences of the inhibition of these additional kinases are difficult to predict. As a next step and before advancing into pharmacological models (representative compounds of this series showed oral availability in rats[27]), we characterized a couple of advanced compounds (**5**, **46**, **47i**, **47l**, and **47p**) in a chemical genomics approach. This approach allowed a further insight into possible cellular on-target as well as off-target effects (even beyond those derived from the inhibition of additional kinases). Results of these studies will be reported in due course.[28]

Conclusions

Potent TGFβRI-selective compounds hold promise for the treatment of pulmonary fibrosis or cancer and additional PDGFRα inhibition could conribute to an attractive target profile. 6-Amido-substituted indolinones are potent inhibitors of the TGFβRI kinase. Selectivity of the compounds against other kinases is generally high (judged on a selectivity panel including 30 representative kinases). The high degree of selectivity may be attributed to the 6-amido moiety pointing toward the kinase selectivity pocket of TGFβRI. Depending on the particular compound substitution pattern, additional PDGFRα-inhibition is achievable. In contrast to many other known TGFβR inhibitors, particularly, p38 kinase is not inhibited by the indolinones. Optimization of an initial lead furnished several compounds with inhibitory potencies against TGFβR1 in the single-digit nanomolar range. For compounds with favorable lipophilicity, biochemical potency translated well into good cellular efficacy, as exemplified by inhibition of Smad2/3 phosphorylation in HaCaT cells. Advanced compounds have been further profiled in a 232-kinase selectivity panel and showed low cross-reactivities within the human kinome.

Experimental Section

All starting materials[18,29,30,31] and reagents were either commercially available or their synthesis had been described in the literature before. All purchased chemicals and solvents were used without further purification. Reaction progresses were usually monitored by TLC using Merck silica gel 60 F_{254} plates and UV light at 254 nm. All chromatographic purifications were conducted as MPLC using DAVISIL LC60A silica gel (35−70 μm) unless otherwise noted. Yields refer to purified products and were not optimized. ^{1}H NMR (400 MHz) spectra were recorded on a Bruker DPX 400 spectrometer using DMSO-d_6 as solvent and $Si(CH_3)_4$ as an internal standard. Low resolution mass spectra (MS) were run on a Micromass platform mass spectrometer. High resolution masses (HRMS) were determined on a Micromass Q-Tof-2 mass spectrometer. The purity of the tested compounds was determined by HPLC and was usually >95%. HPLC retention times were recorded on a Waters 1515 apparatus using a X-Terra MS18 column (2.5 μM, 4.6 mm × 30 mm) eluted with a 3.1 min gradient from 5% to 98% B, wherein A = water/0.1% formic acid and B = acetonitrile/0.1% formic acid.

(*Z*)-3-[Phenyl-(4-piperidin-1-ylmethyl-phenylamino)-methylene]-2-*oxo*-2,3-dihydro-1*H*-indole-6-carboxylic Acid Ethylamide (35). (*Z*)-2-*oxo*-3-[Phenyl-(4-piperidin-1-ylmethyl-phenylamino)-methylene]-2,3-dihydro-1*H*-indole-6-carboxylic acid[18] **23** (400 mg, 0.88 mmol) was suspended in DMF (15 mL) and *N*,*N*′-carbonyldiimidazole (172 mg, 1.06 mmol) was added. The mixture was stirred for 14 h at 80 °C. After that time, the mixture was slowly added to a saturated solution of ethylamine in DMF (15 mL) at −10 °C. Stirring was continued for 2 h at ambient temperature. After that time, the solvent was removed by evaporation, and the residue was purified by column chromatography (silica gel) eluting with methylene chloride/methanol (5/1) to give 47% of **35**. ^{1}H NMR: δ 1.06 (t, 3H), 1.20−1.50 (m, 6H), 2.20 (m, 4H), 3.24 (m, 2H, superimposed on H_2O), 3.28 (s, 2H), 5.72 (d, 1H), 6.76 (d, 2H), 7.04 (m, 3H), 7.33 (s, 1H), 7.40−7.65 (m, 5H), 8.18 (t, 1H), 10.88 (s, 1H), 12.12 (d, 1H). MS: *m*/*z* 481 $[M + H]^+$. HRMS (ES+) calcd for $C_{30}H_{32}N_4O_2$ $[M + H]^+$ *m*/*e* 481.2598, found *m*/*e* 481.2592.

(*Z*)-3-[Phenyl-(4-piperidin-1-ylmethyl-phenylamino)-methylene]-2-*oxo*-2,3-dihydro-1*H*-indole-5-carboxylic Acid Dimethylamide (46). (*Z*)-2-*oxo*-3-[Phenyl-(4-piperidin-1-ylmethyl-phenylamino)-methylene]-2,3-dihydro-1*H*-indole-5-carboxylic acid **22** (640 mg, 1.41 mmol), TBTU (900 mg, 2.80 mmol), HOBt (430 mg, 3.19 mmol), and diethyl-isopropylamine (2.6 g, 2.02 mmol) were suspended in DMF (20 mL) and stirred for 0.5 h at ambient temperature. After that time, dimethylamine hydrochloride (340 mg, 4.20 mmol) was added and stirring was continued for 20 h at ambient temperature. The solvent was partially removed by evaporation and water was added. The precipitate was filtered off to give 600 mg (89%) of **46**. ^{1}H NMR: δ 1.30−1.50 (m, 6H), 2.78 (s, 6H) superimposed on 2.82 (m, 2H), 3.20 (m, 2H), 4.06 (s, 2H), 5.86 (s, 1H), 6.82 (m, 3H), 7.02 (d, 1H), 7.23 (d, 2H), 7.45−7.65 (m, 5H), 10.95 (s, 1H), 12.08 (s, 1H). MS: *m*/*z* 481 $[M]^+$. HRMS (ES+) calcd for $C_{30}H_{32}N_4O_2$ $[M + H]^+$ *m*/*e* 481.2598, found *m*/*e* 481.2591.

General Procedure for the Synthesis of Final Products: (*Z*)-3-({4-[(2-Dimethylaminoethyl)-methanesulfonyl-amino]-phenylamino}-phenyl-methylene)-2-*oxo*-2,3-dihydro-1*H*-indole-6-carboxylic Acid Ethylamide (47a). (*E*)-3-(Hydroxy-phenyl-methylene)-2-*oxo*-2,3-dihydro-1*H*-indole-6-carboxylic acid ethylamide **11** (200 mg, 0.65 mmol) was dissolved in THF (3.0 mL) and *N*-(4-aminophenyl)-*N*-(2-dimethylaminoethyl)-methanesulfonamide[18] (502 mg, 1.95 mmol, 3 equiv) and trimethylsilylimidazole (0.48 mL, 3.25 mmol, 5 equiv) were added. The mixture was stirred for 15 min at 170 °C under microwave irradiation. After that time, the solvent was removed and ethyl acetate was added. The organic layer was washed with water twice and dried over sodium sulfate. The solvent was removed by evaporation, and the residue was triturated with diethylether, filtered off and dried in vacuum at 90 °C to give 210 mg (59%) of **47a**. ^{1}H NMR: δ 1.06 (t, 3H), 2.04 (s, 6H), 2.13 (t, 2H), 2.92 (s, 3H), 3.22 (m, 2H), 3.58 (t, 2H), 5.77 (d, 1H), 6.84 (d, 2H), 7.08 (d, 1H), 7.16 (d, 2H), 7.34 (s, 1H), 7.50−7.60 (m, 5H), 8.15 (t, 1H), 10.82 (s, 1H), 12.14 (s, 1H). MS: *m*/*z* 548 $[M + H]^+$. HRMS (ES+) calcd for $C_{29}H_{33}N_5O_4S$ $[M + H]^+$ *m*/*e* 548.2326, found *m*/*e* 548.2316.

(*Z*)-3-[(4-Dimethylaminomethyl-aminophenyl)-phenyl-methylene]-2-*oxo*-2,3-dihydro-1H-indole-6-carboxylic Acid Ethylamide (47i). Synthesized according to the general procedure

using 4-dimethylaminomethyl-phenylamine[18] and (*E*)-3-(hydroxy-phenyl-methylene)-2-*oxo*-2,3-dihydro-1*H*-indole-6-carboxylic acid ethylamide **11**. Yield: 77% of **47i**. ^{1}H NMR: δ 1.06 (t, 3H), 2.04 (s, 6H), 3.18 (m, 2H) superimposed on 3.20 (s, 2H), 5.71 (d, 1H), 6.77 (d, 2H), 7.04 (m, 3H), 7.32 (s, 1H), 7.46 (m, 2H), 7.54 (m, 3H), 8.13 (t, 1H), 10.84 (s, 1H), 12.09 (s, 1H). MS: *m*/*z* 441 $[M + H]^+$. HRMS (ES+) calcd for $C_{27}H_{28}N_4O_2$ $[M + H]^+$ *m*/*e* 441.2285, found *m*/*e* 441.2277.

(*Z*)-3-[(4-Ethylaminomethyl-aminophenyl)-phenyl-methylene]-2-*oxo*-2,3-dihydro-1*H*-indole-6-carboxylic Acid *N*-Methyl-Ethylamide Trifluoroacetate (47l). (*Z*)-Ethyl-[4-({[6-(ethyl-methyl-carbamoyl)-2-*oxo*-1,2-dihydro-indol-3-ylidene]-phenyl-methyl}-amino)-benzyl]-carbamic acid *tert*-butyl ester **50** (170 mg, 0.306 mmol) was dissolved in methylene chloride (20 mL) and trifluoro-acetic acid (0.5 mL, 6.5 mmol) was added at 0 °C. The mixture was stirred for 1 h at 0 °C and for 12 h at ambient temperature. After that time, the organic phase was washed with water (2×) and dried over sodium sulfate. The solvent was removed by evaporation to give 170 mg (98%) of **47l**. ^{1}H NMR: δ 1.04 (t, 3H), 1.16 (t, 3H), 2.85 (s, 3H), 2.91 (q, 2H), 3.25 (q, 2H, superimposed on H_2O), 4.00 (s, 2H), 5.79 (d, 1H), 6.57 (d, 1H), 6.85 (d, 2H) superimposed on 6.88 (s, 1H), 7.25 (d, 2H), 7.51 (m, 2H), 7.59 (m, 3H), 8.60 (br, 2H), 10.83 (s, 1H), 12.10 (s, 1H). MS: *m*/*z* 455 $[M + H]^+$. HRMS (ES+) calcd for $C_{28}H_{30}N_4O_2$ $[M + H]^+$ *m*/*e* 455.2441, found *m*/*e* 455.2436.

(*Z*)-3-{[4-(2-Dimethylaminoethyl)-aminophenyl]-phenyl-methylene}-2-*oxo*-2,3-dihydro-1*H*-indole-6-carboxylic Acid *N*-Methyl-Ethylamide (47p). Synthesized according to the general procedure using 4-(2-dimethylamino-ethyl)-phenylamine[30] and (*E*)-3-(hydroxy-phenyl-methylene)-2-*oxo*-2,3-dihydro-1*H*-indole-6-carboxylic acid *N*-methyl-ethylamide **10**. Yield: 180 mg (50%) of **47p**. ^{1}H NMR: δ 1.04 (t, 3H), 2.11 (s, 6H), 2.38 (t, 2H), 2.56 (t, 2H), 2.85 (s, 3H), 3.25 (q, 2H, superimposed on H_2O), 5.76 (d, 1H), 6.56 (d, 1H), 6.73 (d, 2H), 6.85 (s, 1H), 7.00 (d, 2H), 7.47 (m, 2H), 7.56 (m, 3H), 10.79 (s, 1H), 12.09 (s, 1H). MS: *m*/*z* 469 $[M + H]^+$. HRMS (ES+) calcd for $C_{29}H_{32}N_4O_2$ $[M + H]^+$ *m*/*e* 469.2598, found *m*/*e* 469.2590.

(*Z*)-3-[(4-Piperidin-1-ylmethyl-phenylamino)-methylene]-2-*oxo*-2,3-dihydro-1*H*-indole-6-carboxylic Acid Ethylamide (47y). Synthesized according to the general procedure using 4-piperi-din-1-ylmethyl-phenylamine[18] and (*E*)-3-hydroxymethylene-2-*oxo*-2,3-dihydro-1*H*-indole-6-carboxylic acid ethylamide **15**. Yield: 26% of **47y**. ^{1}H NMR: δ 1.11 (t, 3H), 2.30−2.50 (m, 6H), 2.31 (m, 4H), 3.24 (m, 2H, superimposed on H_2O), 3.39 (s, 2H), 7.30 (d, 2H), 7.36 (m, 3H), 7.47 (d, 1H), 7.62 (d, 1H), 8.28 (t, 1H), 8.67 (d, 1H), 10.63 (s, 1H), 10.82 (d, 1H). MS: *m*/*z* 405 $[M + H]^+$. HRMS (ES+) calcd for $C_{24}H_{28}N_4O_2$ $[M + H]^+$ *m*/*e* 405.2285, found *m*/*e* 405.2282.

TGFβRI- and PDGFRα IC_{50} Determinations. The inhibition of the kinase activity of TGFβRI was determined using the Promega Kinase-Glo kit (Promega, Mannheim, Germany) according to the manufacturer's protocol in the presence of 600 nM ATP. N-terminally his-tagged human TGFβRI (aa 162-end) expressed in baculovirus and purified using nickel affinity chromatography was used at a final concentration of 0.03 μg/mL. The inhibition of the kinase activity of PDGFRα was determined using the Z′-LYTE assay technology from Invitrogen (Invitrogen Corporation, Carlsbad, CA, USA) according to the manufacturer's protocol. Full-length human PDGFRα (5.6 nM per assay) and the Tyr4 peptide (2 μM per assay) were obtained from Invitrogen, too. IC_{50} values were determined by the use of the Graph PadPrism software.

Phospho-Smad ELISA Assay. HaCaT cells were cultured in DMEM (Gibco, Invitrogen Corporation, Carlsbad, CA, USA) containing 5% FCS. Cells starved for 3 h in DMEM containing no FCS were preincubated with increasing compound concentrations (3.2 nM to 50 μM) or vehicle (DMSO) for 15 min and subsequently stimulated with 5 ng/mL of TGF-βI (R&D System, Minneapolis, MN, USA). After 60 min, cells were washed with ice cold PBS and lysed with 100 μL of cell lysis buffer (Cell Signaling, Danvers, MA, USA) supplemented with 1 mM PMSF (Sigma-Aldrich, St. Louis, MO, USA).

96-Well plates (Nunc MaxiSor, Rochester, NY, USA) were coated with anti-Smad2/3 monoclonal antibody (1 μg/mL; BD Bioscience, San Jose, CA, USA) for 24 h at 4 °C. To reduce unspecific binding, the wells were rinsed with PBS + 0.1% Tween 20 and blocked with PBS + 2% BSA for 2 h at room temperature. After washing three times with PBS + 0.1% Tween 20, the protein lysate was added and incubated for 2 h at room temperature. Wells were washed three times and incubated with an antiphoshpo-Smad2/3 rabbit antisera (Eurogentec, Liege, Belgium) diluted in PBS + 0.2% BSA + 0.02% Tween 20, and incubated for 2 h at room temperature. An AP-conjugated mAb mouse anti rabbit IgG (Sigma-Aldrich, St. Louis, MO, USA) was added and incubated for 2 h at room temperature. Finally, after washing, pNPP liquid substrate system (Sigma-Aldrich, St. Louis, USA) was added and developed in the dark at 37 °C for 2 h before the absorbance was measured at 405 nm in a Synergy HT plate reader (BioTek, Winooski, VT, USA).

Cytotoxicity Assay. The high-content cytotoxicity assay (kit I) was performed according to the manufacturer's instructions (Cellomics, ThermoFisher, Waltham, MA, USA). HaCaT cells were cultured overnight in black 96-well plates, incubated for 24 h with each compound at different concentrations, and stained with cytotoxicity cocktail. Cells were fixed, washed, and scanned on the Cellomics ArrayScan II platform. Images were analyzed with the Cell Health image analysis algorithm. Cytotoxicity indices were calculated for each of the four parameters (cellular membrane integrity, nuclear fragmentation and density, and lysosomal mass) to indicate the percentage of cells outside of the normal range which was defined using a vehicle-treated reference cell population.

Acknowledgment. We thank Stephanie Isambert, Simone Linke, and Josef Zeiler for their excellent technical expertise in the synthesis of the compounds.

Supporting Information Available: Kinase selectivity patterns for compounds **5** and **47i**, the description of the X-ray structure of compound **5** soaked into the TGFβRI kinase domain (shown in Figure 1), as well as additional experimental and spectroscopic data. This material is available free of charge via the Internet at http://pubs.acs.org.

References

(1) (a) Shi, Y.; Massague, J. Mechanisms of TGF-beta signaling from cell membrane to the nucleus. *Cell* **2003**, *113*, 685–700. (b) Ten Dijke, P.; Goumans, M. J.; Itoh, F.; Itoh, S. Regulation of cell proliferation by Smad proteins. *J. Cell Physiol.* **2002**, *191*, 1–16.

(2) Blobe, G. C.; Schiemann, W. P.; Lodish, H. F. Role of transforming growth factor beta in human disease. *N. Engl. J. Med.* **2000**, *342*, 1350–1358.

(3) Lahn, M.; Kloeker, S.; Berry, B. S. TGF-beta inhibitors for the treatment of cancer. *Expert. Opin. Invest. Drugs* **2005**, *14*, 629–643.

(4) Kang, H. R.; Cho, S. J.; Lee, C. G.; Homer, R. J.; Elias, J. A. Transforming growth factor (TGF)-beta1 stimulates pulmonary fibrosis and inflammation via a Bax-dependent, bid-activated pathway that involves matrix metalloproteinase-12. *J. Biol. Chem.* **2007**, *282*, 7723–7732.

(5) Yingling, J. M.; Blanchard, K. L.; Sawyer, J. S. Development of TGF-beta signalling inhibitors for cancer therapy. *Nature Rev. Drug Discovery* **2004**, *3*, 1011–1022.

(6) Zanini, A.; Chetta, A.; Olivieri, D. Therapeutic perspectives in bronchial vascular remodeling in COPD. *Ther. Adv. Respir. Dis.* **2008**, *2*, 179–187.

(7) Rosendahl, A.; Checchin, D.; Fehniger, T. E.; ten Dijke, P.; Heldin, C. H.; Sideras, P. Activation of the TGF-beta/activin-Smad2 pathway during allergic airway inflammation. *Am. J. Respir. Cell Mol. Biol.* **2001**, *25*, 60–68.

(8) (a) Derynck, R.; Akhurst, R. J.; Balmain, A. TGF-beta signaling in tumor suppression and cancer progression. *Nature Genet.* **2001**, *29*, 117–129. (b) Roman, M. F. Targeting TGFβ-mediated processes in cancer. *Curr. Opin. Drug Discovery Dev.* **2009**, *12*, 254–263.

(9) (a) Callahan, J. F.; Burgess, J. L.; Fornwald, J. A.; Gaster, L. M.; Harling, J. D.; Harrington, F. P.; Heer, J.; Kwon, C.; Lehr, R.; Mathur, A.; Olson, B. A.; Weinstock, J.; Laping, N. J. Identification of Novel Inhibitors of the Transforming Growth Factor β1 (TGF-β1) Type 1 Receptor (Alk5). *J. Med. Chem.* **2002**, *45*, 999–1001. (b) Byfield, S. D.; Major, C.; Laping, N. J.; Roberts, A. B. SB-505124 Is a Selective Inhibitor of Transforming Growth Factor-β Type I Receptors ALK4, ALK5, and ALK7. *Mol. Pharmacol.* **2004**, *65*, 744–752.
(10) Li, H.-Y.; McMillen, W. T.; Heap, C. R.; McCann, D. J.; Yan, L.; Campbell, R. M.; Mundla, S. R.; King, C.-H. R.; Dierks, E. A.; Anderson, B. D.; Britt, K. S.; Huss, K. L.; Voss, M. D.; Wang, Y.; Clawson, D. K.; Yingling, J. M.; Sawyer, J. S. Optimization of a Dihydropyrrolopyrazole Series of Transforming Growth Factor-β Type I Receptor Kinase Domain Inhibitors: Discovery of an Orally Bioavailable Transforming Growth Factor-β Receptor Type I Inhibitor as Antitumor Agent. *J. Med. Chem.* **2008**, *51*, 2302–2306.
(11) Bonafoux, D.; Chuaqui, C.; Boriack-Sjodin, P. A.; Fitch, C.; Hankins, G.; Josiah, S.; Black, C.; Hetu, G.; Ling, L.; Lee, W.-C. 2-Aminoimidazoles inhibitors of TGF-β receptor 1. *Bioorg. Med. Chem. Lett.* **2009**, *19*, 912–916.
(12) Kapoun, A. M.; Gaspar, N. J.; Wang, Y.; Damm, D.; Liu, Y.-W.; O'Young, G.; Quon, D.; Lam, A.; Munson, K.; Tran, T.-T.; Ma, J. Y.; Murphy, A.; Dugar, S.; Chakravarty, S.; Protter, A. A.; Wen, F.-Q.; Liu, X.; Rennard, S. I.; Higgins, L. S. Transforming Growth Factor-β Receptor Type I (TGFβRI) Kinase Activity but Not p38 Activation Is Required for TGFβRI-Induced Myofibroblast Differentiation and Profibrotic Gene Expression. *Mol. Pharmacol.* **2006**, *70*, 518–531.
(13) Gellibert, F.; Woolven, J.; Fouchet, M.-H.; Mathews, N.; Goodland, H.; Lovegrove, V.; Laroze, A.; Nguyen, V.-L.; Sautet, S.; Wang, R.; Janson, C.; Smith, W.; Krysa, G.; Boullay, V.; de Gouville, A.-C.; Huet, S.; Hartley, D. Identification of 1,5-Naphthyridine Derivatives as a Novel Series of Potent and Selective TGF-β Type I Receptor Inhibitors. *J. Med. Chem.* **2004**, *47*, 4494–4506.
(14) Gellibert, F.; de Gouville, A.-C.; Woolven, J.; Mathews, N.; Nguyen, V.-L.; Bertho-Ruault, C.; Patikis, A.; Grygielko, E. T.; Laping, N. J.; Huet, S. Discovery of 4-{4-[3- (Pyridin-2-yl)-1*H*-pyrazol-4-yl]pyridin-2-yl}-*N*-(tetrahydro-2*H*-pyran-4-yl)benzamide (GW788388): A Potent, Selective, and Orally Active Transforming Growth Factor-β Type I Receptor Inhibitor. *J. Med. Chem.* **2006**, *49*, 2210–2221.
(15) Kim, D.-K.; Jang, Y.; Lee, H. S.; Park, H.-J.; Yoo, Y. Synthesis and Biological Evaluation of 4(5)-(6-Alkylpyridin-2-yl)imidazoles as Transforming Growth Factor-β Type I Receptor Kinase Inhibitors. *J. Med. Chem.* **2007**, *50*, 3143–3147.
(16) Jachimczak, P. TGFβ in cancer and other diseases—AACR special conference in cancer research. *IDrugs* **2006**, *9*, 239–241.
(17) Behringer, H.; Weissauer, H. Zur Darstellung des Oxindol-aldehyds(3) (Oxymethylene-oxindols) und einiger funktioneller Abkömmlinge. *Chem. Ber.* **1952**, *85*, 774–777.
(18) Roth, G. J.; Heckel, A.; Colbatzky, F.; Handschuh, S.; Kley, J.; Lehmann-Lintz, T.; Lotz, R.; Tontsch-Grunt, U.; Walter, R.; Hilberg, F. Design, Synthesis and Evaluation of Indolinones as Triple Angiokinase Inhibitors and the Discovery of a Highly Specific 6-Methoxycarbonyl-Substituted Indolinone (BIBF 1120). *J. Med. Chem.* **2009**, *52*, 4466–4480.
(19) Chaudhary, N. I.; Roth, G. J.; Hilberg, F.; Müller-Quernheim, J.; Prasse, A.; Zissel, G.; Schnapp, A.; Park, J. E. Inhibition of PDGF, VEGF and FGF signalling attenuates fibrosis. *Eur. Respir. J.* **2007**, *29*, 976–985.
(20) Assay conditions as described in ref 18.
(21) (a) Tsuchida, K.; Nakatani, M.; Hitachi, K.; Uezumi, A.; Sunada, Y.; Ageta, H.; Inokuchi, K. Activitin signaling as an emerging target for therapeutic interventions. *Cell Commun. Signaling* **2009**, *7*, 15. (b) Brown, K. A.; Pietenpol, J. A.; Moses, H. L. A tale of two proteins: differential roles and regulation of Smad2 and Smad3 in TGF-beta signaling. *J. Cell. Biochem.* **2007**, *101*, 9–33.
(22) See Experimental Section. For additional details, refer to ref 28.
(23) Trojanowska, M. Role of PDGF in fibrotic diseases and systemic sclerosis. *Rheumatology* **2008**, *47*, v2–v4.
(24) Östman, A. PDGF-receptors—mediators of autocrine tumor growth and regulators of tumor vasculature and stroma. *Cytokine Growth Factor Rev.* **2004**, *15*, 275–286.
(25) Calculated using the ACDLabs Software (version 4.8.3).
(26) Testing performed by Invitrogen Ltd., United Kingdom. For details please refer to www.invitrogen.com.
(27) Pharmacokinetic parameters of compounds **5** and **47p** have been determined in rats (5 μmol/kg po; 1 μmol/kg iv). Compound **5**: CL = 22 mL/min/kg, MRT (iv) = 3.4 h, MRT (po) = 6.8 h, V_{ss} = 4.4 L/kg, F = 39%. Compound **47p**: CL = 24 mL/min/kg, MRT (iv) = 6.9 h, MRT (po) = 8.9 h, V_{ss} = 10.0 L/kg, F = 40%.
(28) Baum, P.; Schmid, R.; Ittrich, C.; Rust, W.; Fundel-Clemens, K.; Siewert, S.; Baur, M.; Mara, L.; Gruenbaum, L.; Eils, R.; Kontermann, R.; Roth, G. J.; Gantner, F.; Schnapp, A.; Park, J. E.; Weith, A.; Quast, K.; Mennerich, D. Phenocopy—a strategy to qualify chemical compounds during Hit-to-Lead and/or Lead Optimization. *PLoS Genetics*, submitted.
(29) Hardy, G. W.; Lowe, L. A.; Mills, G.; Sang, P. Y.; Simpkin, D. S. A.; Follenfant, R. L.; Shankley, C.; Smith, T. W. Peripherally acting enkephalin analogs. 2. Polar tri- and tetrapeptides. *J. Med. Chem.* **1989**, *32*, 1108–1118.
(30) Klinder, K.; Schrader, K.; Middelhoff, B. New and better methods for the synthesis of pharmacologically important amines. XIV. Synthesis of phenethylamines similar to lobeline. *Arch. Pharm.* **1950**, *283*, 184–190.
(31) Ibrahim, E. S.; Montgomerie, A. M.; Sneddon, A. H.; Proctor, G. R.; Green, B. Synthesis of indolo[3,2-*c*]quinolines and indolo-[3,2-*d*]benzazepines and their interaction with DNA. *Eur. J. Med. Chem.* **1988**, *23*, 183–188.